

Hf/Zr Superlattice-Based High- κ Gate Dielectrics with Dipole Layer Engineering for Advanced CMOS

AUTHOR NAMES

Taeyoung Song,^{1,4,*} Sanghyun Kang,^{1,2,4,*} Yu Hsin Kuo¹, Jiayi Chen¹, Lance Fernandes¹, Nashrah Afroze¹, Mengkun Tian¹, Hyoung Won Baac², Changhwan Shin³ and Asif Islam Khan¹

AUTHOR ADDRESS

¹School of Electrical and Computer Engineering, Georgia Institute of Technology, Atlanta, GA, 30332, USA

²Department of Electrical and Computer Engineering, Sungkyunkwan University, Suwon, 16419, Republic of Korea

³School of Electrical Engineering, Korea University, Seoul, 02841, Republic of Korea

⁴These authors contributed equally

KEYWORDS

Ultrathin high- κ , Superlattice, dipole engineering, reliability, RMG process, GAAFET

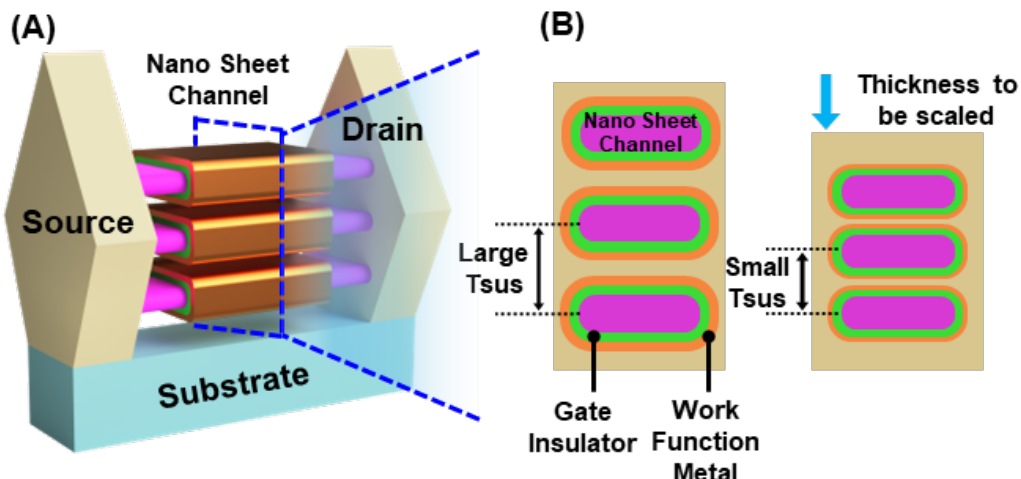
ABSTRACT

Advanced logic transistors require gate dielectrics that achieve sub-nanometer equivalent oxide thickness (EOT), suppress leakage, and satisfy three key requirements: (i) compatibility with RMG-like high-temperature processing, (ii) sufficient V_{th} tunability for multi- V_{th} design, and (iii) high device reliability. However, meeting all of these requirements at once has been difficult with conventional high- κ systems. In this work, we demonstrate that our Hf/Zr-based gate stacks quantitatively satisfy these conditions. (i) After a 700 °C N₂ anneal, the HZH superlattice achieves EOT = 7.3 Å, lower than conventional HfO₂-only stacks (8.5 Å) while maintaining comparable leakage. (ii) Embedding a 3 Å Al₂O₃ dipole within the HfO₂/ZrO₂/HfO₂ superlattice (HZHA) breaks the conventional dipole trade-off, achieving an 8.4 Å EOT—lower than the 9.0 Å of a standard HfO₂/Al₂O₃ stack—while providing a >200 mV V_{FB} shift, thereby enabling multi- V_{th} tuning without compromising scaling. (iii) Furthermore, under -2 V negative-bias temperature stress at 125 °C for 100 s, HZHA and HA exhibit comparable V_{FB} drifts of 87 mV and 97 mV, respectively confirming that strong V_{th} tunability and sub-nanometer EOT can be achieved without compromising stability. In addition to these quantitative advances, this study reveals previously unreported physical insights into dipole behavior and interfacial diffusion in ultrathin Hf/Zr multilayers. These results establish HZHA as an RMG-compatible, V_{th} -tunable, low-EOT dielectric platform capable of supporting logic scaling beyond the 1 nm frontier.

INTRODUCTION

The demand for more powerful and energy-efficient computing, driven by applications in artificial intelligence (AI), high-performance computing, and edge devices, has accelerated the miniaturization of logic transistors. In accordance with Moore's Law, continued scaling to smaller device dimensions improves computational efficiency and integration density, but also

presents new challenges in device design and materials integration. Gate-all-around (GAA) field-effect transistors (FETs) have emerged as a key solution to maintain electrostatic control as transistor width is reduced.¹⁻⁶ Compared to traditional FinFETs, GAA transistors offer superior electrostatic control and reduced short-channel effects, making them well-suited for continued scaling (Figure 1A). By completely wrapping the gate around the channel, GAA FETs suppress short-channel effects and improve performance over traditional FinFETs, enabling further scaling of CMOS technology. However, the relentless drive toward nanometer-scale dimensions imposes severe constraints on integrating critical materials—such as work function metals and gate dielectrics—into an ever-shrinking volume (Figure 1B). In particular, gate dielectrics must provide extremely high capacitance in an ultrathin layer while also allowing tunable threshold voltages (V_{th}) to meet performance requirements. Stronger gate electrostatic control is needed to mitigate short-channel effects, and higher gate capacitance is



required to sustain drive current for high-speed operation.⁷⁻¹²

Figure 1. The Need for Ultra-Thin Gate Oxides with High-k Dielectrics and Low Gate Leakage (A) 3D schematic of a GAAFET structure. (B) Cross-sectional view of stacked nanosheets in a GAAFET, highlighting the increasingly constrained space for gate insulators and work function metals in advanced logic transistors.

One approach to achieve high capacitance at reduced thickness is the integration of advanced high- κ dielectric materials. Recent studies have explored laminated and superlattice oxides based on HfO_2 , ZrO_2 , and Hf-Zr mixed oxides (HZO), particularly near the morphotropic phase boundary (MPB), to enable further EOT scaling.¹³⁻¹⁹ While many of these efforts have focused on metal–insulator–metal capacitors for ferroelectric memory or DRAM applications and sometimes metal–oxide–semiconductor (MOS) structures, high-temperature annealing steps are often omitted, raising concerns about thermal stability. In practical CMOS integration, gate dielectrics must withstand subsequent high-temperature processes such as dopant activation or defect annealing without degradation to ensure long-term device reliability. Post-deposition annealing (PDA) is critical for passivating defects and improving material properties; inadequate thermal treatment can leave the dielectric vulnerable to instability under operating conditions. As such, understanding the impact of high-temperature annealing on advanced high- κ gate stacks is essential for their integration into future technology nodes.^{20, 21}

Another key challenge at aggressively scaled EOT is the increase in gate leakage current due to direct tunneling, which can lead to excessive power consumption. An intrinsic trade-off exists between a dielectric's permittivity (κ) and its bandgap. High- κ materials enable a reduction in gate oxide thickness, enhancing electrostatic gate control. However, their relatively low bandgap energies can lead to increased leakage currents under operating conditions.^{22, 23} Therefore, optimizing the κ –bandgap balance is critical to minimizing leakage while maintaining gate capacitance, particularly in the sub-nanometer EOT regime.

Moreover, as physical dimensions shrink, incorporating work function metals to modulate the threshold voltage (V_{th}) becomes increasingly difficult due to limited gate volume. In this context, dipole engineering within the gate stack provides a "volume-less" method for V_{th} tuning. By introducing ultrathin dielectric interlayers with differing oxygen areal densities

(typically at the high- κ /SiO₂ interface), dipoles which shift the flatband voltage (V_{FB}) without adding physical thickness can be formed. Various dipole materials, such as La₂O₃ and Al₂O₃, and their thickness dependence have been extensively studied.²⁴⁻²⁶ However, systematic investigations into the optimal position of the dipole layer within the gate stack remain limited. Strategic placement of dipole layers could provide additional degrees of freedom for precise V_{th} control in highly scaled devices.

In this study, we systematically investigate four gate dielectric stacks—HfO₂-only, HfO₂/ZrO₂/HfO₂ (HZH), ZrO₂/HfO₂/ ZrO₂ (ZH_Z), and HZO/ZrO₂/HZO (HZZ)—to evaluate their impact on EOT and gate leakage current. A high-temperature 700 °C PDA is found to markedly improve flatband voltage stability under negative bias stress (NBS), with the HZH and ZH_Z configurations demonstrating significantly enhanced reliability compared to the conventional HfO₂-only baseline. Furthermore, we systematically explore dipole engineering by incorporating an ultrathin Al₂O₃ layer at various positions within the stack to modulate the threshold voltage. While such Al₂O₃ integration inevitably increases the EOT due to low dielectric constant of Al₂O₃, this drawback is mitigated by employing the HZH structure. Consequently, the optimized HZHA gate stack (HZH with Al₂O₃ dipole) achieves a favorable combination of reduced EOT, maintaining V_{th} tunability, high-temperature process compatibility, and enhanced reliability, positioning it as a strong candidate for future CMOS logic devices. These findings highlight the HZHA gate stack as a promising platform for enabling EOT scaling, threshold voltage control, and long-term reliability in advanced CMOS logic technologies.

RESULT AND DISCUSSION

Investigation of High- κ Gate Stack Structures for Enhanced Capacitance, Leakage Control and Reliability

We first compared the electrical characteristics of three gate stack structures – HfO_2 -only, HZH, and ZHZ – each with the same total thickness but different layer compositions. The MOS capacitors were fabricated following the process flow shown in Figure S1, with the total gate insulator thickness of 21 Å and additional details explained in the TEM and EDS images (Figure S2, S3). Figure 2A illustrates the layer configurations for the HfO_2 reference and the laminated HZH and ZHZ stacks with layer thicknesses in angstroms. Capacitance–voltage (C–V) and gate leakage current density–voltage (J_g –V) measurements were performed to evaluate the performance of these configurations (Figures 2B–G).

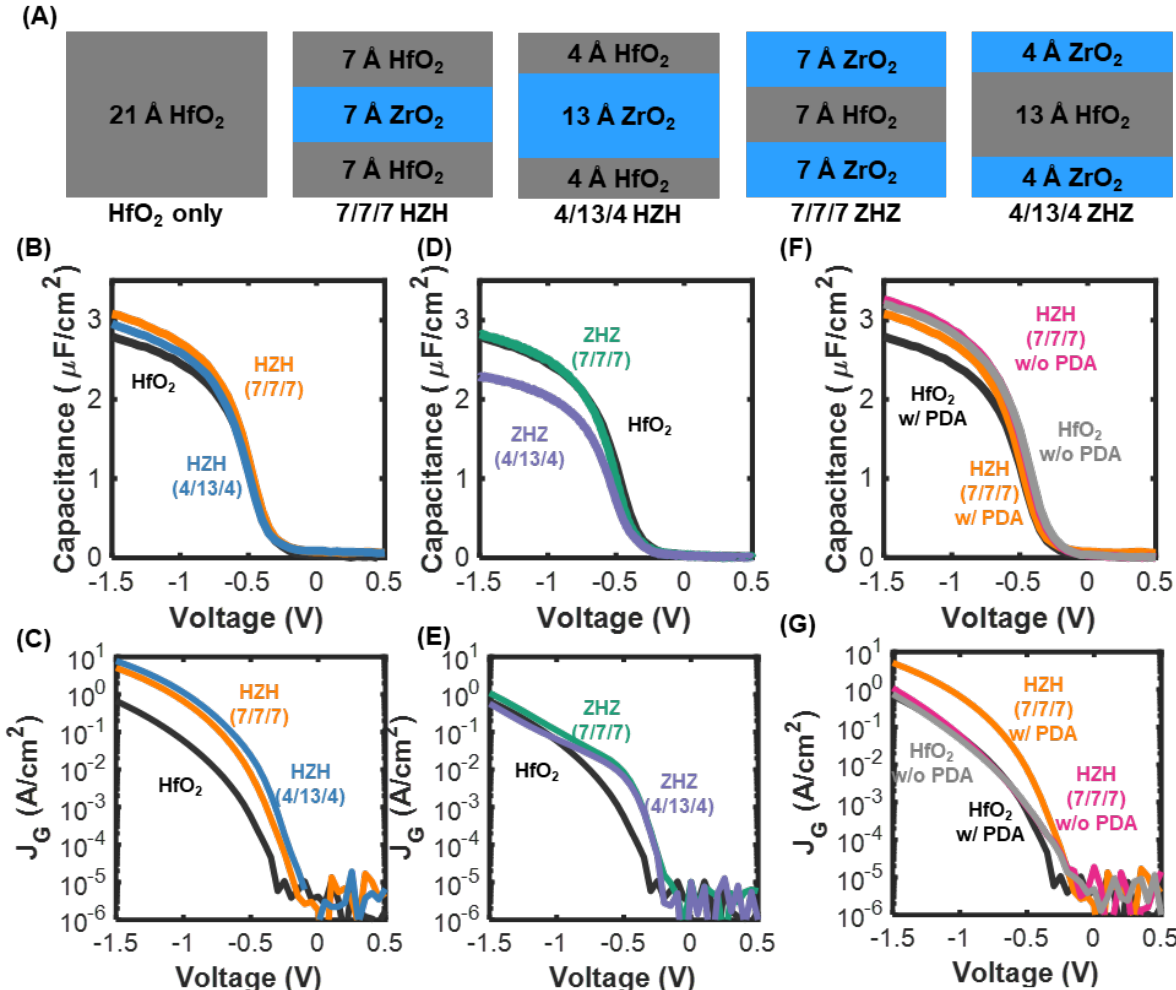


Figure 2. Gate stack engineering for enhanced capacitance and minimized gate leakage current (A) Schematic of the HfO_2 -only, HZH, and ZHZ gate stack configurations with varying thicknesses (B) and (C) Capacitance–voltage (C–V) and gate leakage current–voltage (J_g –V) characteristics of HfO_2 and HZH gate stacks (D) and (E) Capacitance–voltage (C–V) and gate leakage current–voltage (J_g –V) characteristics of HfO_2 and ZHZ gate stacks (F) and (G) Capacitance–voltage (C–V) and gate leakage current–voltage (J_g –V) characteristics of HfO_2 and HZH stacks, both with and without post-deposition annealing (PDA).

This demonstrates that the HZH stack consistently exhibits a higher capacitance than the HfO_2 -only sample, indicating an increased effective dielectric constant due to the incorporation of the intermediate ZrO_2 layer. In contrast, the ZHZ stack shows a capacitance that is comparable to or slightly lower than that of HfO_2 -only, underscoring the strong influence of layer ordering on overall permittivity. Notably, the symmetric 7/7/7 Å HZH laminate achieved an EOT of 7.3 Å, a significant improvement over the 8.5 Å EOT of the HfO_2 -only control. A thicker asymmetric HZH stack (4/13/4 Å) yielded a slightly higher EOT of 7.8 Å, confirming that the HfO_2 : ZrO_2 thickness ratio impacts the dielectric performance. A similar trend is observed in the ZHZ configuration: the symmetric 7/7/7 Å ZHZ stack attained an EOT of 8.4 Å, whereas the less optimized 4/13/4 Å ZHZ stack showed a much larger EOT of 10.6 Å. These results highlight the importance of both the stacking sequence and individual layer thickness optimization in achieving the desired high- κ performance.

Significant research has been devoted to achieving low EOT in HfO_2 - and ZrO_2 -based dielectrics through compositional and structural engineering. Recent studies on ultra-thin ferroelectric HfO_2 – ZrO_2 superlattice capacitors have shown that a coexistence of the ferroelectric orthorhombic (o) phase and the antiferroelectric tetragonal (t) phase can effectively reduce the EOT, leveraging negative capacitance or high permittivity effects at the

phase boundary.^{13, 16, 18} In our HZH laminate, X-ray diffraction (Figure S4) confirms the presence of mixed crystal phases: a dominant o-(111) peak at $2\theta \approx 30.4^\circ$ (accounting for 78.13 % of the film) alongside a weaker t-(011) peak (21.25 %) and a minor monoclinic phase residual. This phase coexistence is a key factor contributing to the reduced EOT of the HZH stack compared to a single-layer HfO_2 film. The ZrO_2 incorporation helps stabilize the desirable orthorhombic phase of HfO_2 , which has higher permittivity, thereby boosting capacitance for a given thickness.

Besides phase stabilization, the $\text{HfO}_2:\text{ZrO}_2$ thickness ratio is pivotal in optimizing dielectric performance. Our comparison of 7/7/7 Å versus 4/13/4 Å HZH stacks shows that the distribution of Hf and Zr dictates the o versus t phase balance and, in turn, the attainable EOT. Sufficient HfO_2 content is required to stabilize the orthorhombic phase; when the ZrO_2 fraction becomes excessive—as in the 4/13/4 Å stack—the structure favors the tetragonal phase, leading to a thicker effective oxide. Precise control of individual layer thicknesses is therefore essential to reproducibly target the desired phase composition and permittivity.

The gate leakage characteristics of the stacks are shown in Figure 2C and 2E. The HZH stack exhibits only a slight increase in leakage current compared to the HfO_2 -only device, while the ZHZ stack maintains a similar leakage level to the HfO_2 reference. This suggests that inserting ZrO_2 layers can enhance capacitance without dramatically compromising leakage current. Leakage current densities in both HZH and ZHZ laminates remain comparable to, or only slightly higher than, those of pure HfO_2 across the operating range, consistent with their band edge alignment: HfO_2 's larger bandgap (~ 5.8 eV) provides the dominant barrier, while the modest introduction of ZrO_2 (~ 5.4 eV) only marginally increases tunneling probability, leaving overall leakage acceptable for logic applications.^{22, 23} However, careful tuning of the ZrO_2 layer's thickness and position is required to balance the trade-off between higher κ and potential increases in leakage. The HZH stack shows a favorable trade-off: it achieves a

substantially lower EOT (higher capacitance) than the HfO₂-only baseline, with only a minor leakage penalty, making it attractive for future high-performance devices. The ZHZ (7/7/7) stack, on the other hand, offers moderate capacitance (similar to HfO₂) but with stable leakage behavior, illustrating how different laminate designs can target either maximum capacitance or minimized leakage according to application needs.

To assess the influence of high temperature processing, we subjected each gate stack to a 700 °C PDA for 30 s in N₂ and compared the results with unannealed controls. Without PDA, the HfO₂ only stack exhibited an exceptionally low EOT of 7.1 Å and low gate leakage. Following the 700 °C anneal, its EOT increased to 8.5 Å and the leakage current rose by roughly 50 % (Figure 2F, G). The HZH stack displayed a more modest EOT shift—from 7.0 Å to 7.3 Å—but experienced a proportionally larger rise in leakage current.

A notable observation in our study is that both EOT and gate leakage current density (J_g) increased after high-temperature annealing even for conventional HfO₂ sample. As 700°C 30s annealing process isn't that high heat budget process enough to transit the phase of crystalline of HfO₂, the primary cause of this degradation is the formation of interfacial silicates at the SiO₂/high-κ interface during annealing. At elevated temperatures, HfO₂ or ZrO₂ in contact with the interfacial SiO₂ layer can react to form hafnium silicate (HfSiO₄) or zirconium silicate (ZrSiO₄). While these silicate phases are thermally stable, they possess a significantly lower dielectric constant than pure HfO₂ or ZrO₂, resulting in an effective thickness increase. Indeed, silicate formation is a well-known limiting factor for EOT scaling in high-κ dielectrics.²⁷ Meanwhile, prior to PDA, the as-deposited EOT values exhibited similar value with best value of HfO₂–ZrO₂ systems from the previous reported paper.¹³ However, after PDA HZH sample would have another effect which is intermixing of HZH and interaction within interface between HfO₂ and ZrO₂ which leads to more increase in the gate leakage.

In our stacks, the ZrO_2 -containing samples were slightly more susceptible to silicate-induced EOT increases than the HfO_2 -only sample. This is expected because ZrSiO_4 formation occurs at a lower temperature than HfSiO_4 .²⁷ Thus, in the ZHZ stack, the bottom ZrO_2 layer can readily convert to ZrSiO_4 at 700 °C, significantly reducing the effective κ at the critical interface. In HZH, the bottom interface is HfO_2 , which is less prone to silicate formation at that temperature, so the EOT penalty is less severe. Consequently, the detrimental impact of silicate formation is more pronounced in the ZHZ structure compared to HZH. Another factor contributing to increased leakage after annealing is grain growth in the polycrystalline HfO_2 and ZrO_2 layers. Prolonged or high temperature anneals can enlarge crystal grains and possibly form grain boundaries that serve as leakage pathways, slightly raising J_g .^{28, 29}

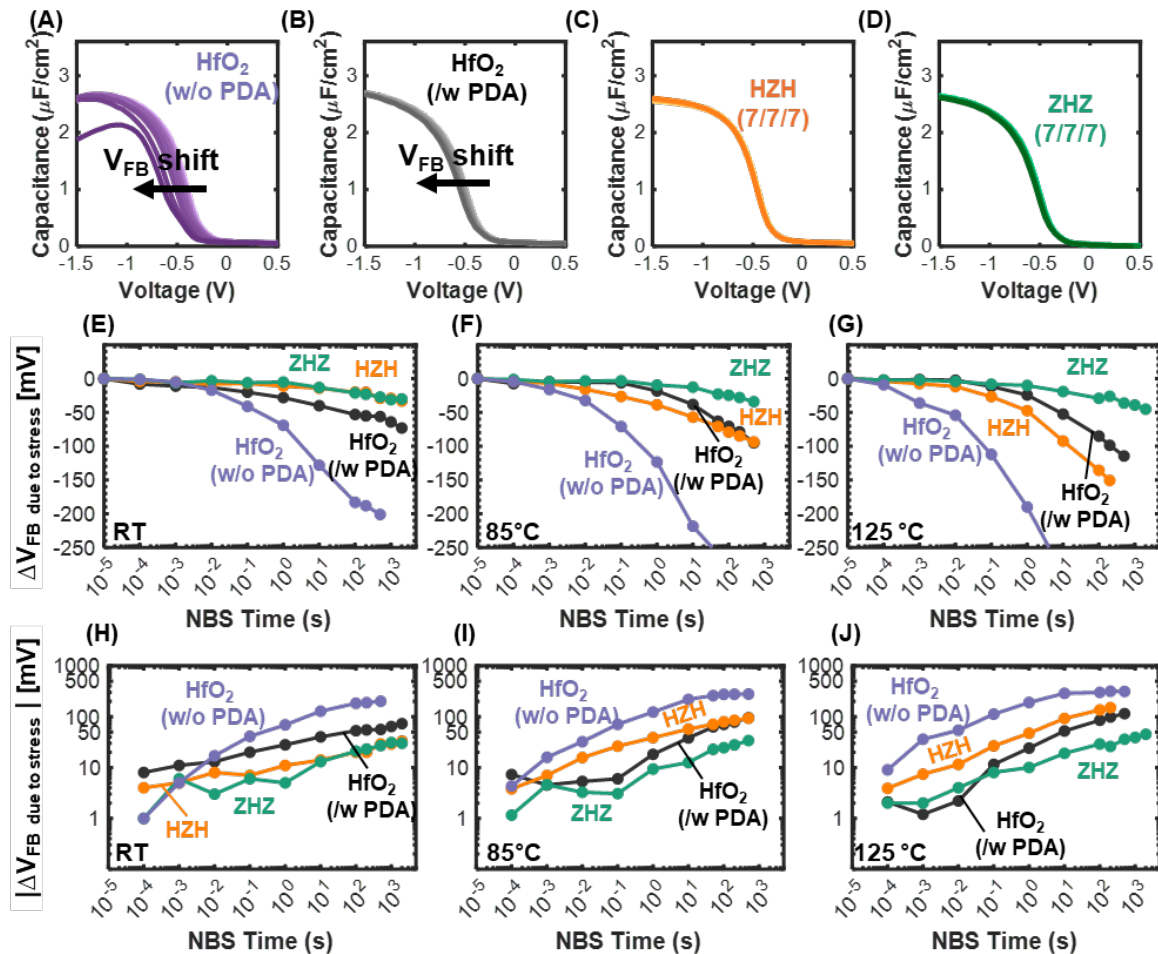


Figure 3. NBS Measurement for Evaluating the Reliability of Various Gate Stacks

(A)–(D) Capacitance-voltage (C–V) measurements under a negative bias (-2V) over a duration of 0 to 2000s. (E)–(G) Flatband voltage shift due to negative bias stress on a linear scale measured at (E) room temperature (RT), (F) 85 °C, and (G) 125 °C. (H)–(J) present the same data on a logarithmic scale at (H) RT, (I) 85 °C, and (J) 125 °C.

We next evaluated the NBS reliability of the gate stacks by measuring the flatband voltage shift under prolonged negative gate bias. MOS capacitors were stressed at -2 V for durations from 1 to 2000 s, and C–V curves were periodically measured to extract V_{FB} (Figure 3A–D). The detailed NBS measurement pulse is illustrated in Figure S6. Tests were done at both room temperature (RT) and an elevated temperature of 85°C and 125 °C to assess thermal acceleration of instability. The unannealed HfO_2 sample showed a pronounced negative V_{FB} shift of -182 mV after just 100 s of stress at RT, indicating substantial charge trapping in the dielectric (primarily hole trapping and interface trap generation).^{30, 31} In contrast, the HfO_2 sample that received the 700 °C PDA exhibited a much smaller shift (-53 mV at 100 s, and -73 mV at 2000 s), highlighting that high-temperature annealing dramatically improves bias stability by reducing pre-existing defects.^{32, 33} This underscores the necessity of PDA in mitigating charge trapping and ensuring long-term reliability of high- κ gate stacks.^{32, 33}

The NBS characteristics further highlight the temperature-dependent reliability differences among the gate stacks. At room temperature, the HZH stack exhibits better NBS stability than the annealed HfO_2 control, while its performance becomes comparable at 85 °C and slightly worse at 125 °C. In contrast, the ZHZ stack maintains consistently superior reliability across all measured temperatures. At RT, the HZH and ZHZ samples exhibit only -33 mV and -30 mV shifts, respectively, after 2000 s of stress. At 125 °C, after 100 s of -2 V stress, annealed HfO_2 shows a -85 mV shift; on the other hand, the HZH and ZHZ stacks exhibit -135 mV and -29 mV shifts, respectively. Even after 2000 s at 125 °C, the ZHZ stack

maintains the smallest degradation (-45 mV). These trends, summarized in Figure 3E–G, indicate that although PDA-treated samples exhibit broadly comparable stability at RT, the ZHZ stack clearly outperforms the others under high-temperature stress. Figures 3H–J present the same data on a logarithmic y-scale. The approximately linear behavior in the log–log plots confirms a power-law dependence of ΔV_{FB} on stress time, consistent with charge-trapping and interface-state generation mechanisms. The activation energies extracted from the Arrhenius analysis of ΔV_{FB} at 100 s (Figure S8) reveal a distinct asymmetry: HZH exhibits a substantially higher E_a whereas both annealed HfO_2 and the ZHZ superlattice show shallow activation energies. This divergence indicates asymmetric $\text{Hf} \leftrightarrow \text{Zr}$ intermixing during high-temperature annealing—pronounced in HZH but strongly suppressed in ZHZ, where the ZrO_2 outer layers act as diffusion barriers. The deeper trap states formed through intermixing in HZH account for its stronger temperature acceleration, whereas the limited intermixing in ZHZ yields shallow trap kinetics and superior high-temperature reliability.

The superior robustness of ZHZ can be understood by examining its initial defect landscape and interfacial chemistry. Silicates such as HfSiO_4 and ZrSiO_4 are known to exhibit lower defect densities than their respective binary oxides.^{34,35} Because ZrSiO_4 forms at a lower temperature than HfSiO_4 ,^{35–37} the ZHZ structure is more likely to develop a ZrSiO_4 -rich transition layer during PDA. This interpretation is strongly supported by the Dit analysis in Figure S7: ZrO_2 -containing stacks exhibit significantly lower Dit after PDA than their HfO_2 counterparts, particularly in the high- ΔE region. Thus, the ZHZ stack begins with a lower density of pre-existing interface traps, reducing the number of sites available for immediate occupation under negative bias. This lower initial trap density plays a decisive role in the early-time NBS response. With fewer traps available for rapid filling, the ZHZ stack shows much smaller ΔV_{FB} shifts during both short and long stress durations. The stress-bias dependence in Figure S9 further supports this conclusion: although ΔV_{FB} increases with both stress voltage

and time, as expected for trap generation under higher fields, the ZHZ stack consistently exhibits the smallest ΔV_{FB} across all bias conditions. Overall, the combination of a lower initial trap density, favorable ZrSiO_4 interfacial formation, and a balanced superlattice arrangement results in the ZHZ gate stack demonstrating the strongest NBS reliability across all temperatures and stress conditions.

In summary, each gate stack configuration offers distinct advantages. The HZH structure provides enhanced capacitance compared to HfO_2 alone, making it appealing for applications that demand high drive current and performance. The ZHZ structure, while not improving EOT beyond the HfO_2 baseline, delivers superior reliability under stress, which is critical for applications requiring long-term stability. These findings underscore the importance of structural engineering in high- κ gate stacks to balance capacitance and leakage performance against reliability.

Impact of Drive-in Temperature on Different Dipole Layer Locations

To systematically study dipole layer placement, we fabricated devices with a 3 Å Al_2O_3 interfacial layer inserted at three different locations in an HfO_2 -based gate stack: at the bottom interface (adjacent to the SiO_2 interfacial layer), in the middle of the HfO_2 , or at the top of the HfO_2 (just below the metal gate). Figure 4A illustrates these configurations. Each of these samples was subjected to anneals at 700 °C, 800 °C, and 900 °C to examine how thermal budget influences dipole formation and activation. The flatband voltage shift (ΔV_{FB}) due to the dipole was extracted from C–V curves for each case (Figure 4B–D).

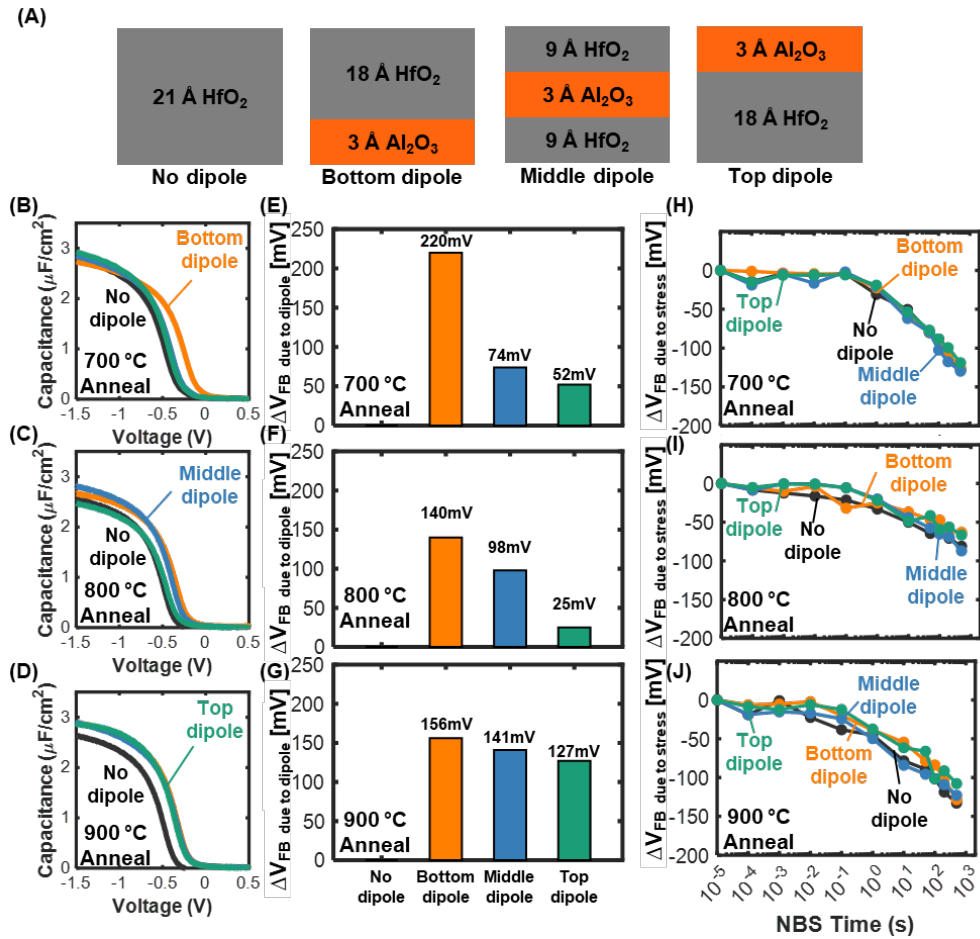


Figure 4. Dipole engineering study with different Al₂O₃ locations and annealing temperatures

(A) Schematic of gate stack configurations with different dipole locations (B)–(D) Capacitance–voltage (C–V) measurements of samples annealed at 700 °C, 800 °C, and 900 °C, respectively (E)–(G) Flatband voltage shift of samples annealed at 700 °C, 800 °C, and 900 °C, respectively (H)–(J) NBS measurement results at elevated temperature (125 °C) for samples annealed at 700 °C, 800 °C, and 900 °C, respectively

At 700 °C, a substantial V_{FB} shift of +220 mV was observed only for the sample with the dipole at the bottom interface, whereas the mid-layer and top-layer dipole samples showed much smaller shifts of +74 mV and +52 mV, respectively (Figure 4E). This behavior indicates that at this relatively lower annealing temperature the dipole is fully activated only when

positioned at the bottom interface, likely because it is directly adjacent to the SiO_2 interface where interfacial dipole formation is most favorable. The corresponding C–V curves (Figure 4B) confirm the large V_{FB} shift for the bottom-dipole device and much less shifts for the other two.

The mechanism of dipole formation at oxide interfaces is rooted in differences in oxygen areal density between two adjoining layers. Generally, when a layer with a higher oxygen concentration is adjacent to one with a lower concentration, oxygen ions tend to diffuse into the lower concentration region upon annealing. This leaves behind oxygen vacancies in the higher concentration material. These oxygen vacancies (positively charged) at the interface align with oxygen anions (negatively charged) in the neighboring layer, thereby forming an electric dipole at the interface. The direction of the dipole depends on the direction of oxygen diffusion.³⁸

In our experiments, we employed Al_2O_3 as the dipole-forming layer. When Al_2O_3 is placed at the bottom of the gate stack (directly on the SiO_2 interfacial layer), oxygen from Al_2O_3 diffuses into SiO_2 during annealing, creating vacancies in Al_2O_3 . This produces dipoles oriented from the SiO_2 side toward the Al_2O_3 , which induces a positive V_{FB} shift.³⁹ By contrast, if the Al_2O_3 layer is located in the middle or top of the HfO_2 stack, it is initially separated from SiO_2 by HfO_2 . Upon annealing, some Al and O interdiffusion can occur through the HfO_2 , and dipoles can still form at the nearest SiO_2 interface. However, the farther the Al_2O_3 is from the SiO_2 , the less oxygen exchange occurs, resulting in a much smaller dipole and hence a smaller V_{FB} shift. This explains why at 700 °C only the bottom dipole showed a significant effect, whereas the middle and top dipoles did not.

When the annealing temperature increased to 800 °C, the dipole in the middle of the stack became more activated, showing a larger ΔV_{FB} of 98 mV, while the bottom dipole's effect slightly decreased to 140 mV (Figure 4F). At 900 °C, the top dipole configuration

exhibited a pronounced V_{FB} shift (127 mV), nearly catching up to ΔV_{FB} of 156 mV with the bottom dipole structure which remained roughly constant between 800 °C and 900 °C as shown in Figure 4G. These trends suggest that higher annealing temperatures enhance the diffusion of oxygen and subsequent dipole formation even for dipoles that are initially farther from the SiO_2 interface. In other words, a sufficiently high-temperature “drive-in” can activate dipole formation throughout the high- κ stack, not just at the bottom interface. To activate dipoles located away from the immediate interface, we used a higher-temperature drive-in anneal (up to 900 °C). At such high temperatures, the diffusion lengths of oxygen in HfO_2 increase substantially, enabling oxygen from Al_2O_3 even in the middle or upper part of the stack to reach the SiO_2 eventually, thereby forming measurable dipoles (Figure 4G).^{24, 40}

Conversely, for the bottom dipole, as the net dipole effect at the bottom interface slightly diminishes beyond 700 °C, there appears to be an optimal annealing window. An intriguing behavior was observed for the bottom dipole case: The V_{FB} shift caused by the bottom Al_2O_3 layer was largest at 700 °C and then reduced at 800 °C and 900 °C. This non-monotonic trend can be understood by considering the so-called mirror-plane effect in high- κ dielectrics. In a HfO_2 -based dielectric stack, there can be a self-regulating interdiffusion of cations and anions at interfaces that tends to neutralize dipoles.²⁵ At moderate temperatures, enough oxygen diffuses to form a strong dipole at the $\text{SiO}_2/\text{Al}_2\text{O}_3$ interface, while Hf and other cation diffusion is limited. At much higher temperatures, however, oxygen diffusion becomes extremely pronounced and can extend beyond the first interface: in our case, oxygen from Al_2O_3 can diffuse not only into SiO_2 but also upward into the adjacent HfO_2 layer. Concurrently, Hf cations can diffuse into the Al_2O_3 region to some extent. This upward anion/cation intermixing generates an opposite interfacial dipole component—i.e., a counter-dipole—that partially cancels the intended dipole at the SiO_2 interface. Specifically, since HfO_2 has a lower oxygen areal density than Al_2O_3 , oxygen will also diffuse from Al_2O_3 into HfO_2 at high

temperature, creating vacancies in Al_2O_3 near the HfO_2 side. This induces an opposing dipole oriented from Al_2O_3 toward HfO_2 .^{38, 41} At 900 °C, this counter-dipole effect remains present but is not strictly monotonic: the net V_{FB} shift is still lower than at 700 °C but slightly higher than at 800 °C, consistent with temperature-dependent competition between dipole formation and counter-dipole cancellation. In summary, these results demonstrate that excessive high-temperature diffusion introduces a counter-dipole that reduces the net dipole strength, and a careful control of the annealing temperature is required to maximize the beneficial dipole at the SiO_2 interface while avoiding excessive counter-dipole formation due to over-diffusion.

We further evaluated the dipole-engineered stacks under negative bias stress (NBS) across multiple temperatures, including room temperature (RT), 85 °C, and 125 °C. The elevated-temperature results at 125 °C are presented in Figure 4H–J, while the corresponding RT and 85 °C data are provided in Figure S10. The NBS pulse conditions were consistent with those described in Figure S6. As expected, applying –2 V stress induced a negative shift in V_{FB} in all cases due to charge trapping. Importantly, however, the magnitude of the V_{FB} shift after stress was similar for devices with bottom, middle, or top dipoles and largely independent of whether they were annealed at 700, 800, or 900 °C. In other words, within the measurement resolution, dipole layer placement and the drive-in anneal temperature did not significantly affect the NBS-induced degradation. All devices showed only modest V_{FB} shifts under prolonged stress, indicating that the introduction of the Al_2O_3 dipole layer does not compromise the reliability of the gate stack.

The impact of dipole insertion on channel mobility and reliability is an important consideration for practical devices. Some studies have reported that if a dipole-forming layer such as Al_2O_3 is directly interfaced with SiO_2 , it can lead to mobility degradation in MOSFETs, possibly due to scattering from the dipole interface.²⁴ Conversely, other reports suggest that dipoles can improve reliability by providing a source of excess oxygen to passivate interface

traps, thereby reducing interface state density (D_{it}).⁴² Our reliability tests on capacitors with various dipole placements (Figure 4H–J) showed no adverse effect of the dipole on NBS-induced V_{FB} shifts even at elevated temperature(125°C) – all configurations were essentially equally stable, and in fact the absolute shifts were very small. This suggests that, at least in terms of bias stress, adding an Al_2O_3 dipole layer does not degrade the dielectric reliability. It will be necessary, however, to conduct bias-temperature instability (BTI) tests on actual transistors to fully evaluate any subtle effects dipoles might have on channel mobility or interface trap generation over operating lifetimes.

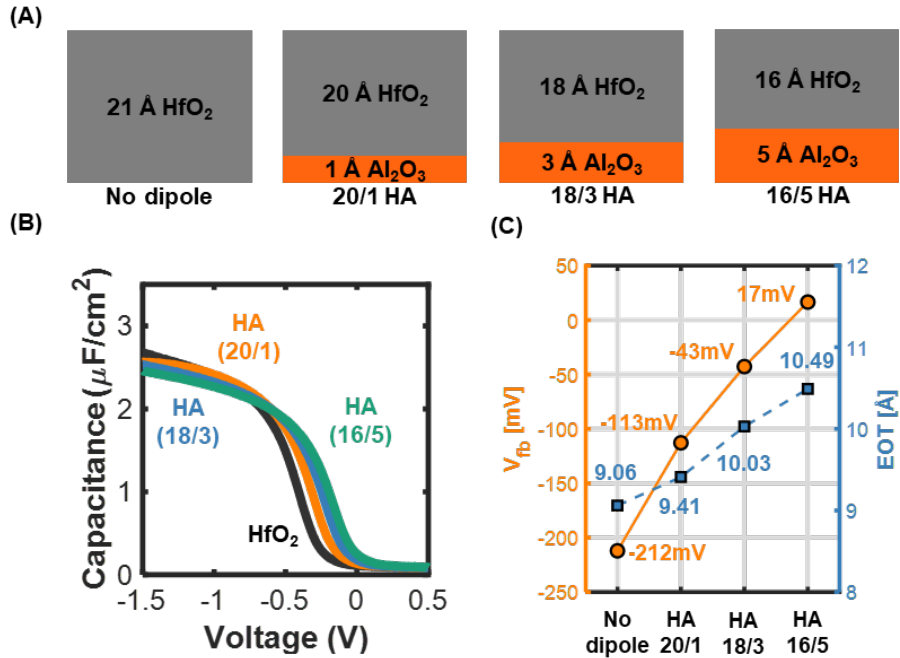


Figure 5. Demonstration of the EOT– V_{FB} shift trade-off by modulating Al_2O_3 dipole thickness in $\text{HfO}_2/\text{Al}_2\text{O}_3$ gate stacks. (A) Schematic of gate stack configurations with different dipole thicknesses (B) Capacitance–voltage (C–V) measurements of HA stacks with varying Al_2O_3 thicknesses (C) Flatband voltage (V_{FB}) and equivalent oxide thickness (EOT) values as a function of Al_2O_3 dipole thickness

To evaluate threshold voltage tunability, we investigated the dependence of electrical characteristics on Al_2O_3 thickness in the gate stack structures, as illustrated in Figure 5A. Three different Al_2O_3 thicknesses, 1 Å, 3 Å, and 5 Å were incorporated by partially replacing the 21 Å HfO_2 layer, ensuring that the total dielectric thickness remained constant across all samples. This approach allowed for a controlled assessment of dipole strength while minimizing capacitance variations caused by total thickness changes. The capacitance–voltage (C–V) measurements (Figure 5B) show a clear positive shift of the C–V curve as the Al_2O_3 thickness increases, accompanied by a decrease in maximum capacitance. The extracted V_{FB} values exhibit a strong correlation with Al_2O_3 thickness (Figure 5C): +99 mV for 1 Å, +169 mV for 3 Å, and +229 mV for 5 Å, confirming that the dipole effect intensifies with increasing Al_2O_3 thickness. This enhancement is attributed to interfacial dipole formation, driven by differences in oxygen areal density between adjacent dielectric layers. Thicker Al_2O_3 layers promote greater oxygen diffusion, resulting in a stronger dipole moment and a larger positive shift in V_{FB} . The EOT values, extracted from the C–V curves (Figure 5C), show a clear degradation trend with increasing Al_2O_3 thickness due to its intrinsically lower dielectric constant compared to HfO_2 . Specifically, EOT increased by 0.35 Å, 0.97 Å, and 1.43 Å for 1 Å, 3 Å, and 5 Å of Al_2O_3 , respectively. These results clearly demonstrate the intrinsic EOT– V_{FB} trade-off in conventional $\text{HfO}_2/\text{Al}_2\text{O}_3$ dipole stacks, motivating the use of intrinsically low-EOT platforms—such as the Hf/Zr superlattice—to enable meaningful V_{th} modulation without compromising scaling. In this context, it is important to evaluate how dipole-based V_{th} implications for advanced CMOS design.

V_{FB} Modulation in Superlattice High- κ Gate Stacks through Dipole Engineering

To investigate the effect of incorporating an Al_2O_3 dipole into previously examined gate stack structures, we embedded the dipole layer into $\text{HfO}_2/\text{ZrO}_2$ superlattice configurations. By doing so, we leverage the enhanced permittivity of the laminate while gaining the V_{FB} modulation of the dipole, thus balancing electrostatic control with capacitance retention. We extended our investigation beyond the HfO_2 -only dielectric to three laminated high- κ stacks (HZH, ZHZ, and HZZ), each incorporating a bottom-interface Al_2O_3 dipole (Figure 6A).

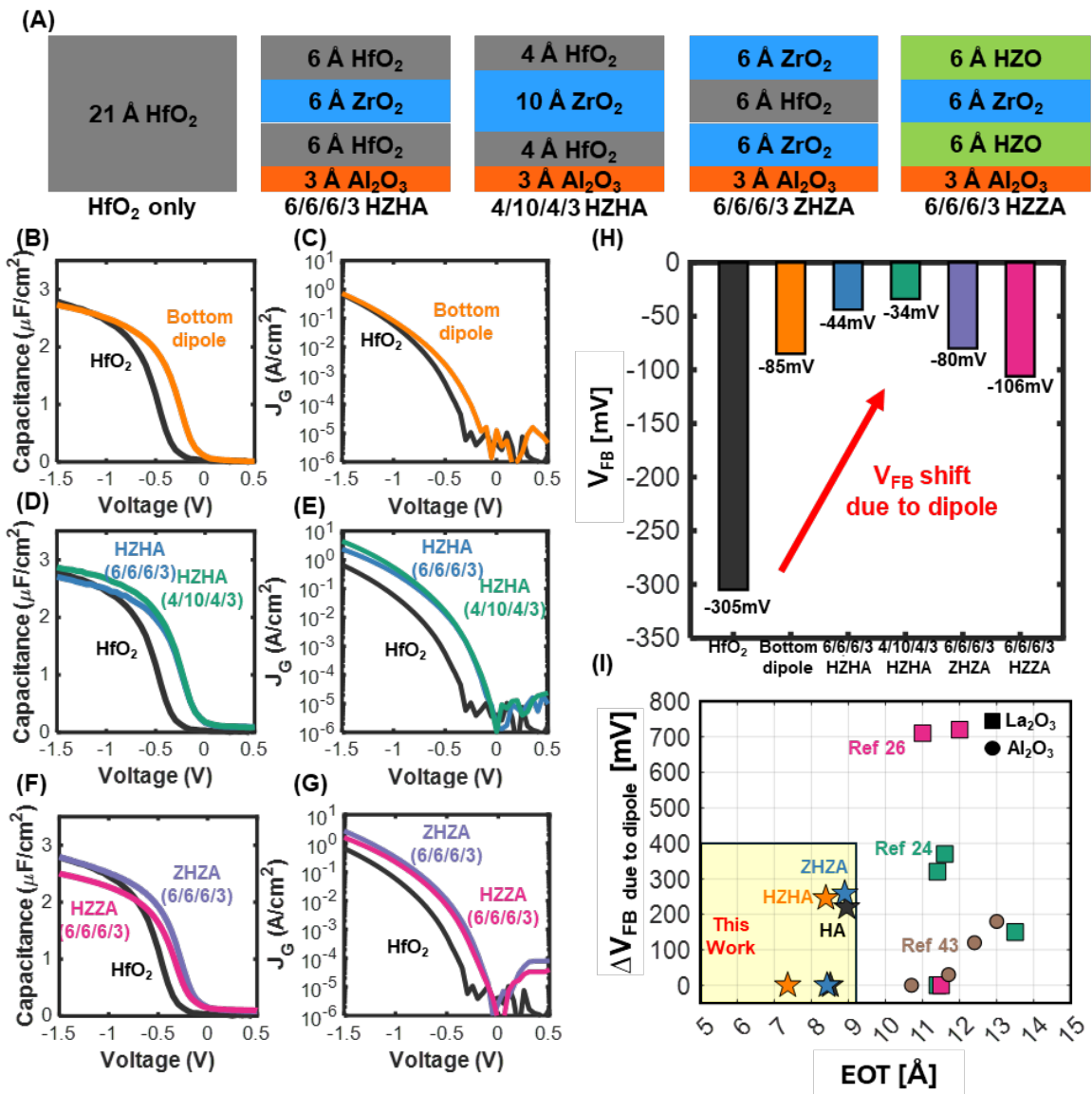


Figure 6. Incorporation of a dipole into the Hf/Zr Superlattice structure for V_{th} tunability and enhanced high- κ performance (A) Schematic of the HfO_2 -only, HZH, ZHZ, and HZZ gate stack configurations with the dipole layer positioned at the bottom. (B) and (C) Capacitance–voltage (C – V) and gate leakage current–voltage (J_g – V) characteristics for HfO_2 and HfO_2 with a bottom dipole. (D) and (E) Capacitance–voltage (C – V) and gate leakage current–voltage (J_g – V) characteristics for HfO_2 and HZH gate stacks with a bottom dipole. (F) and (G) Capacitance–voltage (C – V) and gate leakage current–voltage (J_g – V) characteristics for HfO_2 and ZHZ/HZZ gate stacks with a bottom dipole. (H) Flatband voltage of different gate stacks. Regardless of the gate stack configuration, those incorporating a bottom dipole exhibit a flatband voltage shift. (I) Benchmark comparison of the studied gate stacks with results from other studies.

Figure 6B–G presents C – V and J_g – V data for several representative cases with a bottom dipole. The introduction of the 3 Å Al_2O_3 layer at the $\text{HfO}_2/\text{SiO}_2$ interface consistently induces a positive flatband voltage shift, confirming the formation of the intended dipole. Quantitatively, adding the dipole to a pure HfO_2 gate stack (sample “HA,” referring to HfO_2 + bottom dipole Al_2O_3) shifted V_{FB} by about +220 mV relative to the undoped HfO_2 , but also increased the EOT from 8.5 Å to 9.0 Å. Importantly, the gate leakage current density remained essentially unchanged by the dipole (Figure 6B, C). This demonstrates that the Al_2O_3 interlayer can modulate V_{th} without incurring a severe leakage penalty, although a slight capacitance reduction is observed.

The stack composition with the dipole significantly influences the overall device behavior. Among the high- κ laminates tested, the HZH stack showed the lowest EOT even with the dipole in place—even slightly lower than the conventional HfO_2 without a dipole. In contrast, the ZHZ stack with a dipole exhibited a lower capacitance and higher leakage

compared to its no-dipole counterpart, underlining that the base $\text{HfO}_2/\text{ZrO}_2$ configuration can matter as much as the dipole itself. We further examined two HZH stack variants with different $\text{HfO}_2/\text{ZrO}_2$ thickness ratios to see how they interact with the dipole. Without a dipole, the symmetric 7/7/7 HZH had a lower EOT than the asymmetric 4/13/4 HZH, as discussed earlier. When the dipole was added at the bottom interface, an interesting result emerged: the 4/10/4/3 HZHA stack achieved a lower EOT (8.4 Å) than the 6/6/6/3 HZHA stack (9.2 Å). In other words, the laminate with a higher ZrO_2 proportion benefitted more from the dipole integration in terms of maintaining a low EOT. By contrast, other dipole-integrated configurations like ZHZA ($\text{ZrO}_2/\text{HfO}_2/\text{ZrO}_2 + \text{Al}_2\text{O}_3$) and HZZA ($\text{HZO}/\text{ZrO}_2/\text{HZO} + \text{Al}_2\text{O}_3$) exhibited significantly higher EOTs (8.9 Å and 10.0 Å, respectively) despite the dipole, due to their less favorable base structures. These findings emphasize that to fully exploit dipole engineering, one must jointly optimize the high- κ stack geometry. A well-tuned $\text{HfO}_2:\text{ZrO}_2$ ratio can offset the intrinsic EOT cost of the Al_2O_3 layer, thereby maximizing capacitance while still enabling V_{FB} shifts.

We calculated the flatband voltages for all the different gate stacks to compare the effect of the dipole (Figure 6H). In each case, incorporating the Al_2O_3 dipole resulted in a discernible V_{FB} shift relative to the corresponding structure without a dipole. The magnitude of the shift varied depending on the stack composition (with HZH showing the largest shift and HZZ the smallest), but the qualitative presence of a shift in HZH, ZHZ, and HZZ confirms successful dipole formation in all these high- κ matrices. This demonstrates the versatility of dipole engineering across various dielectric heterostructures; even when the baseline V_{FB} of HZH, ZHZ, and pure HfO_2 devices are nearly identical, adding the dipole reliably moves V_{FB} in the positive direction.

Figure 6I provides a performance benchmarking of our dipole-integrated stacks in terms of flatband voltage shift (ΔV_{FB}) versus EOT.⁴³ As noted, the HfO_2 -only + dipole stack

(HA) incurs a slight EOT increase compared to pure HfO_2 . In contrast, the HZH + dipole stack manages to achieve a lower EOT than pure HfO_2 due to the ZrO_2 layers while still obtaining a sizable ΔV_{FB} shift from the dipole. This underlines the promise of combining laminate high- κ dielectrics with dipole layers: the laminate addresses the capacitance requirement, and the dipole provides V_{th} tuning, with manageable trade-offs.

Figure 6I benchmarks the flat-band voltage tunability (ΔV_{FB}) against equivalent oxide thickness for various dipole-engineered gate stacks reported in the literature. Prior studies employing La_2O_3 or Al_2O_3 interlayers have demonstrated substantial ΔV_{FB} (>300 – 700 mV) but at the cost of large EOTs (20–50 Å). In contrast, our HfO_2 – ZrO_2 superlattice platform enables the integration of a 3 Å Al_2O_3 dipole within sub-10 Å EOT stacks: the HZHA and ZHZA structures both exhibit ΔV_{FB} shifts in excess of 200 mV while maintaining EOTs of 8.4 Å and 9.0 Å, respectively. This performance region (highlighted in yellow) lies well below the EOT regime of previous dipole-only approaches, illustrating that coupling dipole engineering with high- κ superlattice dielectric stacks is a highly effective strategy to achieve aggressive scaling and threshold-voltage tunability simultaneously.

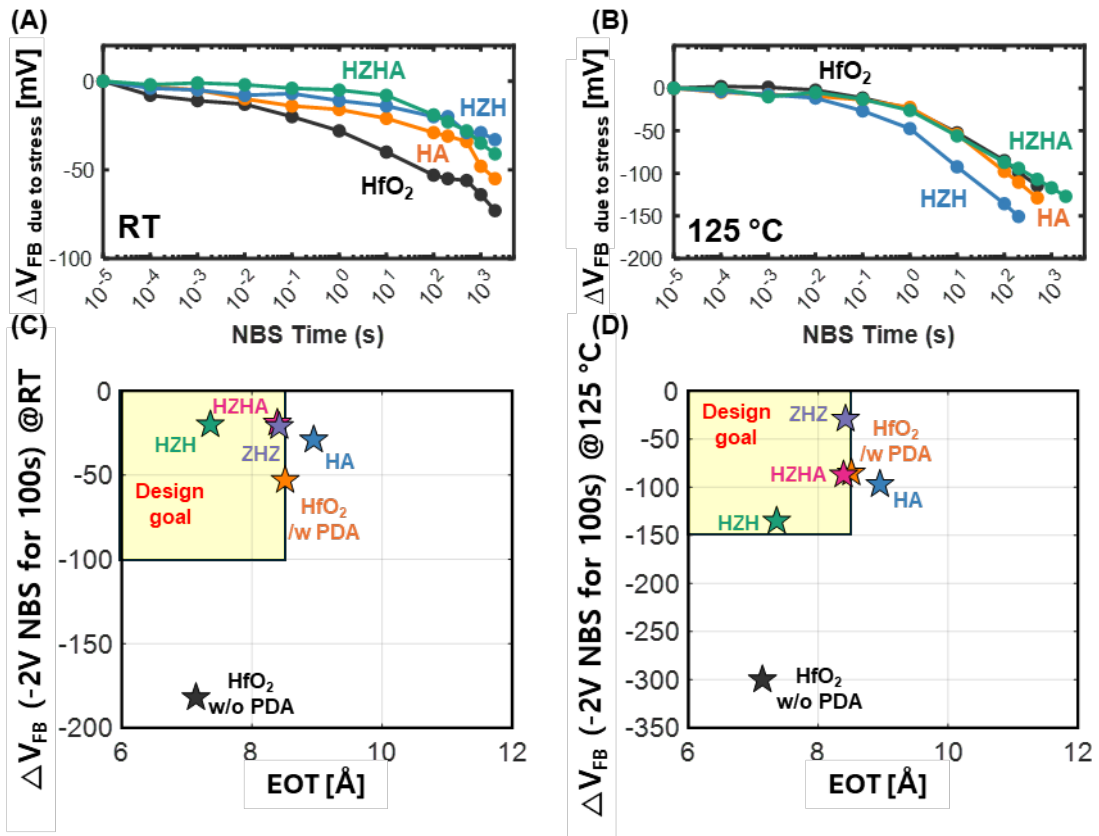


Figure 7. NBS measurements of gate stacks with incorporated dipole layer

(A) and (B) Flatband voltage shift (ΔV_{FB}) as a function of negative bias stress (NBS) time measured at room temperature and 125 °C for various gate stack configurations. (C) and (D) Flatband voltage shift (V_{FB}) versus EOT plot for the structures investigated in this work.

We further evaluated the NBS reliability of these dipole-integrated superlattice stacks. Figure 7A–B compares the NBS response of four stacks—HfO₂, HA, HZH, and HZHA—at room temperature and 125 °C. At both temperatures, introducing an ultrathin Al₂O₃ dipole directly on the SiO₂ interlayer (HA) does not degrade reliability; the ΔV_{FB} versus time trace remains similar to, or modestly better than, that of the conventional HfO₂. This behavior suggests that the dipole interface supplies excess oxygen during stress, promoting partial conversion of HfO₂ to Hf-Al silicate and thereby passivating vacancy sites that would

otherwise trap holes. When the dipole is embedded within the $\text{HfO}_2/\text{ZrO}_2/\text{HfO}_2$ superlattice (HZHA), the stack retains the superlattice's intrinsic NBS robustness at room temperature and, importantly, sustains comparable or slightly smaller ΔV_{FB} than conventional HfO_2 at 125 °C. The combination of Zr-mediated trap suppression and Al-assisted interfacial silicate formation therefore enables the HZHA architecture to deliver threshold voltage tunability without sacrificing high temperature reliability, affirming its suitability for advanced CMOS logic applications. Figure 7C–D plots the 100 s negative-bias stress ΔV_{FB} against EOT for all investigated stacks at room temperature and 125 °C respectively. The shaded “design goal” region denotes the quadrant combining $\text{EOT} < 8.5 \text{ \AA}$ with $|V_{FB}| < 100 \text{ mV}$. At both temperatures, the HZHA stack lies within this target region, exhibiting an EOT of 8.4 Å alongside minimal ΔV_{FB} (< 20 mV at RT and < 100 mV at 125 °C). For comparison, the HA stack provides tunability but falls outside the design window because of its larger EOT, whereas the conventional HfO_2 stack without PDA exhibits a substantial flatband voltage shift. Notably, HZHA maintains low ΔV_{FB} under high-temperature stress—demonstrating that embedding the dipole within the $\text{HfO}_2\text{--ZrO}_2$ superlattice uniquely satisfies the competing requirements of sub-nanometer scaling and robust negative-bias reliability. In parallel, our NBS data highlight the strong potential of the ZHZ architecture for applications requiring enhanced reliability under both thermal and electrical stress. By naturally forming a more inert interface and maintaining a high overall κ , the ZHZ stack achieves an excellent balance of performance and stability. It points to a broader strategy where interface chemistry is engineered for reliability in tandem with bulk high- κ improvements.

Finally, by incorporating an Al_2O_3 dipole into our best-performing high- κ laminates (HZH, ZHZ, HZZ), we demonstrated clear flatband voltage modulation in each case (Figure 6H). The fact that the baseline V_{FB} of HZH, ZHZ, and HZZ without dipole could be made nearly identical through appropriate metal gate work function, and then each could be shifted

positively by adding the dipole, confirms the viability of dipole engineering across different high- κ systems. The dipole did incur a minor EOT due to a lower dielectric constant of Al_2O_3 than that of HfO_2 and ZrO_2 ,^{22, 23} but the leakage current remained largely unchanged. Notably, the HZHA (4/10/4/3) stack achieved a slightly lower EOT than even some no-dipole configurations, illustrating that a well-optimized $\text{HfO}_2/\text{ZrO}_2$ composition can compensate for the Al_2O_3 's lower κ . This implies that by tuning the Hf:Zr ratio in concert with dipole integration, one can simultaneously maximize the dipole effect and minimize the EOT penalty, ultimately preserving or even enhancing the overall capacitance.

Table 1 synthesizes the key performance metrics of the investigated gate stacks—EOT, gate leakage density, flatband voltage shifts after negative bias stress at both room temperature and 125 °C, V_{th} tunability, and compatibility with replacement metal gate (RMG) processing. Relative to the HfO_2 control, HZH superlattices deliver thinner EOTs without sacrificing significant leakage integrity, and the 700 °C post-deposition anneal substantially suppresses NBS-induced V_{FB} drift. Incorporating an ultrathin Al_2O_3 dipole layer increases EOT for any stack; however, the high- κ HZH framework offsets this penalty, such that the dipole-integrated HZHA stack retains competitive EOT while gaining intrinsic V_{th} adjustability. Moreover, HZHA maintains NBS stability at elevated temperature and endures the high temperature anneal, confirming full compatibility with advanced RMG flows. Collectively, the data position HZHA as the most balanced candidate for future logic nodes, combining aggressive scaling, threshold voltage control, and robust reliability.

Gate stack	HfO ₂ only	HfO ₂ only	HZH	HZH	ZHZ	HA	HZHA
	w/o PDA	/w PDA	w/o PDA	/w PDA	/w PDA	/w PDA	/w PDA
							
EOT [Å]	7.1	8.5	7.0	7.3	8.4	9.0	8.4
J_g @V_{FB} -1V [A/cm²]	0.20	0.31	0.28	2.36	0.59	0.64	0.68
V_{FB} shift due to NBS @100s at RT [mV]	-182	-53	N/A	-20	-21	-29	-19
V_{FB} shift due to NBS @100s at 125°C [mV]	-300	-85	N/A	-135	-29	-97	-87
V_{th} tunability	X	X	X	X	X	✓	✓
RMG process compatibility	X	✓	X	✓	✓	✓	✓

Table 1. Summary table of characteristics for various types of gate stacks

Table 2 benchmarks MFIS gate-stack performance reported in prior studies, comparing annealing conditions, EOT/CET, and V_{th} tunability. The color coding indicates CMOS process compatibility, with green representing the most favorable conditions, yellow indicating intermediate performance, and red indicating the least favorable outcome. Notably, the gate dielectric developed in this work withstands high-temperature annealing up to 700 °C while still achieving a low EOT enabled by the HfO₂/ZrO₂ superlattice structure. Furthermore, the incorporation of an ultrathin Al₂O₃ dipole layer within the superlattice allows controllable

V_{FB} tuning, demonstrating that both aggressive EOT scaling and threshold-voltage engineering can be simultaneously realized within a CMOS-compatible thermal budget.

Ref.	Structure	PDA (post-deposition annealing)			PMA (post-metallization annealing)			EOT [Å]	CET [Å]	V_{th} tunability		
		T_{ox}	Temp	Time	Ambient	Temp	Time	Ambient				
This Work	HZH	700 °C	30 s	N2	-			/w PDA 7.3	-	✓		
	21 Å				-			w/o PDA 7.0				
13	HZH	175 °C	20 m	FGA	175 °C	20 m	FGA	6.5	-	X		
	20 Å				-			-				
16	HZO	-			600 °C	spike	-	12	-	X		
	25 Å	-			450 °C			-				
44	HZO	-			500 °C	30 s	-	-	-	X		
	15 Å	-			500 °C			-				
45	HZO	-			500 °C	30 s	-	-	-	X		
	60 Å	-			500 °C			-				
46	HZO	-			500 °C	30 s	N ₂	-	-	X		
	100 Å	-			500 °C			-				
47	HZO	-			600 °C	30 s	Ar	-	9.8	X		
	50 Å	-			600 °C			-				
48	HZO	250 °C	-	-	450 °C	60 s	N ₂	-	-	X		
	24 Å	-			450 °C			-				

Table 2. Benchmark table of MFIS gate-stack performance against state-of-the-art works, comparing annealing conditions, EOT/CET, and V_{th} tunability. Color coding qualitatively benchmarks CMOS compatibility: green is most favorable, yellow is intermediate, and red is least favorable.

CONCLUSION

In this work, we demonstrate that $\text{HfO}_2/\text{ZrO}_2$ superlattice gate stacks incorporating ultrathin Al_2O_3 dipole layers simultaneously achieve aggressive EOT scaling, low leakage, tunable flat-band voltage, and high-temperature CMOS compatibility. The optimized HZH laminate delivers a 7.3 Å EOT—well below the 8.5 Å of conventional HfO_2 —while dipole integration enables >200 mV V_{FB} modulation with an 8.4 Å EOT in the HZHA stack. Although ZHZ does not further reduce EOT, it exhibits outstanding negative-bias stress resilience, reducing the 125 °C ΔV_{FB} from 85 mV (HfO_2) to 29 mV. In addition to these device-level

advances, the study reveals two previously unreported physical insights—position-dependent dipole activation with a high-temperature counter-dipole response, and asymmetric $\text{Hf} \leftrightarrow \text{Zr}$ intermixing that dictates trap energetics—offering new understanding of dipole formation, ionic diffusion, and defect behavior in ultrathin high- κ heterostructures. Collectively, these results position dipole-engineered $\text{HfO}_2/\text{ZrO}_2$ superlattices as a promising pathway toward sub-nanometer, high-performance gate dielectrics for future CMOS nodes.

METHOD

The detailed device fabrication process is described in Note S1, while the device measurement methods for C-V, J_g -V, and NBS are explained in Note S2. Additionally, the parameter extraction method for V_{FB} , EOT, and J_g at $V_{FB} - 1\text{V}$ is provided in Note S3.

AUTHOR INFORMATION

Corresponding Author

*T.S. E-mail: tsong77@gatech.edu

* S.K. E-mail: skang415@gatech.edu

Author Contributions

A.K., and C.S. supervised the research. T.S., S.K., and Y.K. designed the research. T.S., S.K., and Y.K. conducted the experiments and analyzed the results. Y.K., J.C., L.F., N.A., and M.T. assisted with the data analysis. T.S., and S.K. wrote the manuscript with input from all authors.

ACKNOWLEDGMENT

This work was supported by SRC GRC 2024 Logic and Memory Devices (#3235.001) and the National Research Foundation of Korea (NRF) grant funded by the Korea government (MSIT)

(No. RS-2023-00260527). We also acknowledge Seunghoon Sung, Ashish Penumatcha, and Uygar Avci of Intel Foundry Technology Research (Hillsboro, OR, USA, and Ireland) for their valuable contributions and insightful discussions.

REFERENCES

- (1) Loubet, N.; Hook, T.; Montanini, P.; Yeung, C. W.; Kanakasabapathy, S.; Guillom, M.; Yamashita, T.; Zhang, J.; Miao, X.; Wang, J.; et al. Stacked nanosheet gate-all-around transistor to enable scaling beyond FinFET. In *2017 Symposium on VLSI Technology*, 2017.
- (2) Ajayan, J.; Nirmal, D.; Tayal, S.; Bhattacharya, S.; Arivazhagan, L.; Fletcher, A. S. A.; Murugapandian, P.; Ajitha, D. Nanosheet field effect transistors-A next generation device to keep Moore's law alive: An intensive study. *Microelectronics Journal* **2021**, *114*. DOI: 10.1016/j.mejo.2021.105141.
- (3) Zhang, Q.; Zhang, Y.; Luo, Y.; Yin, H. New structure transistors for advanced technology node CMOS ICs. *Natl Sci Rev* **2024**, *11* (3), nwae008. DOI: 10.1093/nsr/nwae008 From NLM PubMed-not-MEDLINE.
- (4) Huang, J.; Heh, D.; Sivasubramani, P.; Kirsch, P.; Bersuker, G.; Gilmer, D.; Quevedo-Lopez, M.; Hussain, M.; Majhi, P.; Lysaght, P. Gate first high-k/metal gate stacks with zero SiO x interface achieving EOT= 0.59 nm for 16nm application. In *2009 Symposium on VLSI Technology*, 2009; IEEE: pp 34-35.
- (5) Changhwan, C.; Chang Yong, K.; Se Jong, R.; Abkar, M. S.; Krishna, S. A.; Manhong, Z.; Hyungseob, K.; Tackhwi, L.; Feng, Z.; Injo, O.; et al. Fabrication of TaN-gated ultra-thin mosfets (eot >1.0nm) with HfO2 using a novel oxygen scavenging process for sub 65nm application. In Digest of Technical Papers. *2005 Symposium on VLSI Technology*, 2005., 2005.
- (6) Ando, T.; Frank, M. M.; Choi, K.; Choi, C.; Bruley, J.; Hopstaken, M.; Copel, M.; Cartier, E.; Kerber, A.; Callegari, A.; et al. Understanding mobility mechanisms in extremely scaled HfO2 (EOT 0.42 nm) using remote interfacial layer scavenging technique and Vt-tuning dipoles with gate-first process. In *2009 IEEE International Electron Devices Meeting (IEDM)*, 2009.
- (7) Bao, R.; Durfee, C.; Zhang, J.; Qin, L.; Rozen, J.; Zhou, H.; Li, J.; Mukesh, S.; Pancharatnam, S.; Zhao, K.; et al. Critical Elements for Next Generation High Performance Computing Nanosheet Technology. In *2021 IEEE International Electron Devices Meeting (IEDM)*, 2021.
- (8) Bao, R.; Watanabe, K.; Zhang, J.; Guo, J.; Zhou, H.; Gaul, A.; Sankarapandian, M.; Li, J.; Hubbard, A. R.; Vega, R.; et al. Multiple-Vt Solutions in Nanosheet Technology for High Performance and Low Power Applications. In *2019 IEEE International Electron Devices Meeting (IEDM)*, 2019.
- (9) Zhang, J.; Ando, T.; Yeung, C. W.; Wang, M.; Kwon, O.; Galatage, R.; Chao, R.; Loubet, N.; Moon, B. K.; Bao, R.; et al. High-k metal gate fundamental learning and multi-Vt options for stacked nanosheet gate-all-around transistor. In *2017 IEEE International Electron Devices Meeting (IEDM)*, 2017.
- (10) Bao, R.; Zhou, H.; Wang, M.; Guo, D.; Haran, B. S.; Narayanan, V.; Divakaruni, R. Extendable and Manufacturable Volume-less Multi-Vt Solution for 7nm Technology Node and Beyond. In *2018 IEEE International Electron Devices Meeting (IEDM)*, 2018.
- (11) Yao, J.; Wei, Y.; Yang, S.; Yang, H.; Xu, G.; Zhang, Y.; Cao, L.; Zhang, X.; Liu, Q.; Wu, Z.; et al. Record 7(N)+7(P) Multiple VTs Demonstration on GAA Si Nanosheet n/pFETs using

WFM-Less Direct Interfacial La/Al-Dipole Technique. In 2022 International Electron Devices Meeting (IEDM), 2022.

(12) Chang, V. S.; Wang, S. H.; Lu, J. H.; Wu, W. H.; Wu, B. F.; Hsu, B. C.; Kwong, K. C.; Yeh, J. Y.; Chang, C. H.; Chen, C. H.; et al. Enabling Multiple-Vt Device Scaling for CMOS Technology beyond 7nm Node. In 2020 IEEE Symposium on VLSI Technology, 2020.

(13) Cheema, S. S.; Shanker, N.; Wang, L. C.; Hsu, C. H.; Hsu, S. L.; Liao, Y. H.; San Jose, M.; Gomez, J.; Chakraborty, W.; Li, W.; et al. Ultrathin ferroic HfO(2)-ZrO(2) superlattice gate stack for advanced transistors. *Nature* **2022**, *604* (7904), 65-71. DOI: 10.1038/s41586-022-04425-6 From NLM PubMed-not-MEDLINE.

(14) Li, W.; Wang, L. C.; Cheema, S. S.; Shanker, N.; Park, J. H.; Liao, Y. H.; Hsu, S. L.; Hsu, C. H.; Volkman, S.; Sikder, U.; et al. Demonstration of Low EOT Gate Stack and Record Transconductance on $L_{\text{g}}=90$ nm nFETs Using 1.8 nm Ferroic HfO₂-ZrO₂ Superlattice. In 2021 IEEE International Electron Devices Meeting (IEDM), 2021.

(15) Shanker, N.; Wang, L.-C.; Cheema, S.; Li, W.; Choudhury, N.; Hu, C.; Mahapatra, S.; Salahuddin, S. On the PBTI Reliability of Low EOT Negative Capacitance 1.8 nm HfO₂-ZrO₂ Superlattice Gate Stack on $L_{\text{g}}=90$ nm nFETs. In 2022 IEEE Symposium on VLSI Technology and Circuits (VLSI Technology and Circuits), 2022.

(16) Ni, K.; Saha, A.; Chakraborty, W.; Ye, H.; Grisafe, B.; Smith, J.; Rayner, G. B.; Gupta, S.; Datta, S. Equivalent Oxide Thickness (EOT) Scaling With Hafnium Zirconium Oxide High- κ Dielectric Near Morphotropic Phase Boundary. In 2019 IEEE International Electron Devices Meeting (IEDM), 2019.

(17) Gaddam, V.; Kim, G.; Kim, T.; Jung, M.; Kim, C.; Jeon, S. Novel Approach to High kappa (approximately 59) and Low EOT (approximately 3.8 Å) near the Morphotropic Phase Boundary with AFE/FE (ZrO₂/HZO) Bilayer Heterostructures and High-Pressure Annealing. *ACS Appl Mater Interfaces* **2022**, *14* (38), 43463-43473. DOI: 10.1021/acsami.2c08691 From NLM PubMed-not-MEDLINE.

(18) Zhou, J.; Zhou, Z.; Jiao, L.; Wang, X.; Kang, Y.; Wang, H.; Han, K.; Zheng, Z.; Gong, X. Al-doped and Deposition Temperature-engineered HfO₂ Near Morphotropic Phase Boundary with Record Dielectric Permittivity (~68). In 2021 IEEE International Electron Devices Meeting (IEDM), 2021.

(19) Lou, Z. F.; Chen, B. R.; Hsiang, K. Y.; Chang, Y. T.; Liu, C. H.; Tseng, H. C.; Liao, H. T.; Su, P.; Lee, M. H. Super-Lamination HZO/ZrO₂/HZO of Ferroelectric Memcapacitors With Morphotropic Phase Boundary (MPB) for High Capacitive Ratio and Non-Destructive Readout. *IEEE Electron Device Letters* **2024**, *45* (12), 2355-2358. DOI: 10.1109/led.2024.3485916.

(20) Linder, B. P.; Dasgupta, A.; Ando, T.; Cartier, E.; Kwon, U.; Southwick, R.; Wang, M.; Krishnan, S. A.; Hopstaken, M.; Bajaj, M.; et al. Process optimizations for NBTI/PBTI for future replacement metal gate technologies. In 2016 IEEE International Reliability Physics Symposium (IRPS), 2016.

(21) Mertens, H.; Ritzenthaler, R.; Arimura, H.; Franco, J.; Sebaai, F.; Hikavyy, A.; Pawlak, B. J.; Machkaoutsan, V.; Devriendt, K.; Tsvetanova, D.; et al. Si-cap-free SiGe p-channel FinFETs and gate-all-around transistors in a replacement metal gate process: Interface trap density reduction and performance improvement by high-pressure deuterium anneal. In 2015 Symposium on VLSI Technology (VLSI Technology), 2015.

(22) Clark, R. D. Emerging Applications for High K Materials in VLSI Technology. *Materials (Basel)* **2014**, *7* (4), 2913-2944. DOI: 10.3390/ma7042913 From NLM PubMed-not-MEDLINE.

(23) Wilk, G. D.; Wallace, R. M.; Anthony, J. M. High- κ gate dielectrics: Current status and materials properties considerations. *Journal of Applied Physics* **2001**, *89* (10), 5243-5275. DOI: 10.1063/1.1361065.

(24) Arimura, H.; Ragnarsson, L. A.; Oniki, Y.; Franco, J.; Vandooren, A.; Brus, S.; Leonhardt, A.; Sippola, P.; Ivanova, T.; Verni, G. A.; et al. Dipole-First Gate Stack as a Scalable and Thermal Budget Flexible Multi-Vt Solution for Nanosheet/CFET Devices. In 2021 IEEE International Electron Devices Meeting (IEDM), 2021.

(25) Zheng, D.; Chung, W.; Chen, Z.; Si, M.; Wilk, C.; Ye, P. D. Controlling Threshold Voltage of CMOS SOI Nanowire FETs With Sub-1 nm Dipole Layers Formed by Atomic Layer Deposition. *IEEE Transactions on Electron Devices* **2022**, *69* (2), 851-856. DOI: 10.1109/ted.2021.3136493.

(26) Wei, Y.; Yao, J.; Zhang, Q.; Sang, G.; Bao, Y.; Gao, J.; Li, J.; Luo, J.; Yin, H. Sub-5-Å La₂O₃ In Situ Dipole Technique for Large VFB Modulation With EOT Reduction and Improved Interface for HKMG Technology. *IEEE Transactions on Electron Devices* **2024**, *71* (1), 746-751. DOI: 10.1109/ted.2023.3335900.

(27) Wilk, G. D.; Wallace, R. M.; Anthony, J. M. Hafnium and zirconium silicates for advanced gate dielectrics. *Journal of Applied Physics* **2000**, *87* (1), 484-492. DOI: 10.1063/1.371888.

(28) Kim, S.; Lee, S. H.; Kim, M. J.; Hwang, W. S.; Jin, H. S.; Cho, B. J. Method to Achieve the Morphotropic Phase Boundary in HfxZr_{1-x}O₂ by Electric Field Cycling for DRAM Cell Capacitor Applications. *IEEE Electron Device Letters* **2021**, *42* (4), 517-520. DOI: 10.1109/led.2021.3059901.

(29) Onaya, T.; Nabatame, T.; Sawamoto, N.; Ohi, A.; Ikeda, N.; Chikyow, T.; Ogura, A. Improvement in ferroelectricity of HfxZr_{1-x}O₂thin films using ZrO₂seed layer. *Applied Physics Express* **2017**, *10* (8). DOI: 10.7567/apex.10.081501.

(30) Jeppson, K. O.; Svensson, C. M. Negative bias stress of MOS devices at high electric fields and degradation of MNOS devices. *Journal of Applied Physics* **1977**, *48* (5), 2004-2014. DOI: 10.1063/1.323909.

(31) Stathis, J. H.; Zafar, S. The negative bias temperature instability in MOS devices: A review. *Microelectronics Reliability* **2006**, *46* (2-4), 270-286. DOI: 10.1016/j.microrel.2005.08.001.

(32) Chatterjee, S.; Kuo, Y.; Lu, J.; Tewg, J. Y.; Majhi, P. Electrical reliability aspects of HfO₂ high-k gate dielectrics with TaN metal gate electrodes under constant voltage stress. *Microelectronics Reliability* **2006**, *46* (1), 69-76. DOI: 10.1016/j.microrel.2005.02.004.

(33) He, G.; Liu, M.; Zhu, L. Q.; Chang, M.; Fang, Q.; Zhang, L. D. Effect of postdeposition annealing on the thermal stability and structural characteristics of sputtered HfO₂ films on Si (100). *Surface Science* **2005**, *576* (1-3), 67-75. DOI: 10.1016/j.susc.2004.11.042.

(34) Cho, M.; Kaczer, B.; Kauerauf, T.; Ragnarsson, L.-A.; Groeseneken, G. Improved NBTI reliability with sub-1-nanometer EOT ZrO₂ gate dielectric compared with HfO₂. *IEEE Electron Device Letters* **2013**, *34* (5), 593-595. DOI: 10.1109/led.2013.2253755.

(35) Shin, D.; Liu, Z.-K. Phase stability of hafnium oxide and zirconium oxide on silicon substrate. *Scripta Materialia* **2007**, *57* (3), 201-204. DOI: 10.1016/j.scriptamat.2007.04.011.

(36) Puthenkovilakam, R.; Carter, E. A.; Chang, J. P. First-principles exploration of alternative gate dielectrics: Electronic structure of ZrO₂/Si and ZrSiO₄/Si interfaces. *Physical Review B* **2004**, *69* (15). DOI: 10.1103/PhysRevB.69.155329.

(37) Chen, T.-J.; Kuo, C.-L. First principles study of the oxygen vacancy formation and the induced defect states in hafnium silicates. *Journal of Applied Physics* **2012**, *111* (7). DOI: 10.1063/1.3702578.

(38) Kita, K.; Toriumi, A. Origin of electric dipoles formed at high-k/SiO₂ interface. *Applied Physics Letters* **2009**, *94* (13). DOI: 10.1063/1.3110968.

(39) Iwamoto, K.; Kamimuta, Y.; Ogawa, A.; Watanabe, Y.; Migita, S.; Mizubayashi, W.; Morita, Y.; Takahashi, M.; Ota, H.; Nabatame, T.; et al. Experimental evidence for the flatband voltage shift of high-k metal-oxide-semiconductor devices due to the dipole formation at the high-k/SiO₂ interface. *Applied Physics Letters* **2008**, *92* (13). DOI: 10.1063/1.2904650.

(40) Zhang, Y.; Choi, M.; Wang, Z.; Choi, C. Dipole formation to modulate flatband voltage using ALD Al₂O₃ and La₂O₃ at the interface between HfO₂ and Si or Ge substrates. *Applied Surface Science* **2023**, *609*. DOI: 10.1016/j.apsusc.2022.155295.

(41) Lv, Y.-D.; Shen, L.; Li, Y.-C.; Shi, C.-Y.; Huang, Z.-Y.; Yu, X.; Zhu, X.-N.; Lu, H.-L.; Yu, S.; Zhang, D. W. Atomic-Layer-Deposited Al₂O₃ Layer Inserted in SiO₂/HfO₂ Gate-Stack-Induced Positive Flat-Band Shift with Dual Interface Dipoles for Advanced Logic Device. *ACS Applied Nano Materials* **2024**, *7* (24), 28496-28503. DOI: 10.1021/acsanm.4c05649.

(42) Rignanese, G. M.; Gonze, X.; Jun, G.; Cho, K.; Pasquarello, A. First-principles investigation of high- κ dielectrics: Comparison between the silicates and oxides of hafnium and zirconium. *Physical Review B* **2004**, *69* (18). DOI: 10.1103/PhysRevB.69.184301.

(43) Morooka, T.; Matsuki, T.; Mise, N.; Kamiyama, S.; Nabatame, T.; Eimori, T.; Nara, Y.; Ohji, Y. Improvement of Device Characteristics for TiN Gate p-Type Metal–Insulator–Semiconductor Field-Effect Transistor with Al₂O₃-Capped HfO₂ Dielectrics by Controlling Al₂O₃ Diffusion Annealing Process. *Japanese Journal of Applied Physics* **2009**, *48* (4S). DOI: 10.1143/jjap.48.04c010.

(44) Xu, Q.; Chen, K.; Xu, G.; Xiang, J.; Gao, J.; Wang, X.; Li, J.; He, X.; Li, J.; Wang, W. Physical thickness 1.5-Nm HfZrO negative capacitance nmosfETs. *IEEE Transactions on Electron Devices* **2021**, *68* (7), 3696-3701.

(45) Kim, S.; Kim, H. M.; Kwon, K. R.; Kwon, D. Stacked Nanosheet Gate-All-Around Morphotropic Phase Boundary Field-Effect Transistors. *Advanced Science* **2025**, *12* (18), 2413090.

(46) Sharma, P.; Zhang, J.; Saha, A.; Gupta, S.; Datta, S. Negative capacitance transients in metal-ferroelectric Hf 0.5 Zr 0.5 O 2-Insulator-Semiconductor (MFIS) capacitors. In *2017 75th Annual Device Research Conference (DRC)*, 2017; IEEE: pp 1-2.

(47) Lee, M.; Chen, P.-G.; Liu, C.; Chu, K.; Cheng, C.-C.; Xie, M.-J.; Liu, S.-N.; Lee, J.-W.; Huang, S.-J.; Liao, M.-H. Prospects for ferroelectric HfZrO_x FETs with experimentally CET= 0.98 nm, SS_{for}= 42mV/dec, SS_{rev}= 28mV/dec, switch-off< 0.2 V, and hysteresis-free strategies. In *2015 IEEE international electron devices meeting (IEDM)*, 2015; IEEE: pp 22.25. 21-22.25. 24.

(48) Zhong, K.; Zhang, Z.; Liu, S.; Lyu, H.; Yin, H. Demonstration of EOT-Scaled Lg~ 25 nm FinFET Based on Thickness-Proportion Controlled HfO₂-ZrO₂-HfO₂ Superlattice Gate Stacks. In *2025 9th IEEE Electron Devices Technology & Manufacturing Conference (EDTM)*, 2025; IEEE: pp 1-3.